Nonlinear self-polarization flipping in silicon sub-wavelength waveguides: distortion, loss, dispersion, and noise effects

Wen Qi Zhang,[1,*] **M. A. Lohe,**[1] **Tanya M. Monro,**[1] **Paolo Bettotti,**[2] **Lorenzo Pavesi,**[2] **and Shahraam Afshar V**[1]

[1]*Institute for Photonics & Advanced Sensing, University of Adelaide, SA 5005, Australia*
[2]*Nanoscience Laboratory, Department of Physics, University of Trento, Via Sommarive 14, 38123 Trento, Italy*

[*]*wenqi.zhang@adelaide.edu.au*

Abstract: We numerically investigate nonlinear self-polarization flipping in a silicon waveguide. We identify specific silicon waveguide geometries that enhance this effect to facilitate its fabrication and experimental demonstration by varying various parameters such as fabrication distortion, waveguide loss, dispersion and laser noise to design the silicon waveguide. In optimized waveguides, we show that nonlinear self-polarization flipping can be observed with few tens of watts peak power pulses with widths as short as 60 ps and laser noise level as large as 7%.

OCIS codes: (190.0190) Nonlinear optics; (060.4370) Nonlinear optics, fibers; (060.5530) Pulse propagation and temporal solitons; (230.7370) Waveguides; (230.5440) Polarization-selective devices.

References and links

1. V. R. Almeida, Q. Xu, C. A. Barrios, and M. Lipson, "Guiding and confining light in void nanostructure," Opt. Lett. **29**, 1209–1211 (2004).
2. O. Boyraz, P. Koonath, V. Raghunathan, and B. Jalali, "All optical switching and continuum generation in silicon waveguides," Opt. Express **12**, 4094–4102 (2004).
3. C. Koos, P. Vorreau, T. Vallaitis, P. Dumon, W. Bogaerts, R. Baets, B. Esembeson, I. Biaggio, T. Michinobu, F. Diederich, W. Freude, and J. Leuthold, "All-optical high-speed signal processing with silicon-organic hybrid slot waveguides," Nat. Photonics **3**, 216–219 (2009).
4. W. Astar, J. B. Driscoll, X. Liu, J. I. Dadap, W. M. J. Green, Y. A. Vlasov, G. M. Carter, and R. M.Osgood Jr., "Tunable wavelength conversion by XPM in a silicon nanowire, and the potential for XPM-multicasting," J. Lightwave Technol. **28**, 2499–2511 (2010).
5. R. K. W. Lau, M. Ménard, Y. Okawachi, M. A. Foster, A. C. Turner-Foster, R. Salem, M. Lipson, and A. L. Gaeta, "Continuous-wave mid-infrared frequency conversion in silicon nanowaveguides," Opt. Lett. **36**, 1263–1265 (2011).
6. M. Pelusi, F. Luan, T. D. Vo, M. R. E. Lamont, S. J. Madden, D. A. Bulla, D.-Y. Choi, B. Luther-Davis, and B. J. Eggleton, "Photonic-chip-based radio-frequency spectrum analyser with terahertz bandwidth," Nat. Photonics **3**, 139–143 (2009).
7. X. Gai, T. Han, A. Prasad, S. Madden, D.-Y. Choi, R. Wang, D. Bulla, and B. Luther-Davies, "Progress in optical waveguides fabricated from chalcogenide glasses," Opt. Express **18**, 26635–26646 (2010).
8. B. J. Eggleton, B. Luther-Davies, and K. Richardson, "Chalcogenide photonics," Nat. Photonics **5**, 141–148 (2011).
9. P. Petropoulos, T. M. Monro, W. Belardi, K. Furusawa, J. H. Lee, and D. J. Richardson, "2r-regenerative all-optical switch based on a highly nonlinear holey fiber," Opt. Lett. **26**, 1233–1235 (2001).

#222244 - $15.00 USD Received 5 Sep 2014; accepted 13 Oct 2014; published 31 Oct 2014

10. H. Ebendorff-Heidepriem, P. Petropoulos, S. Asimakis, V. Finazzi, R. C. Moore, K. Frampton, F. Koizumi, D. J. Richardson, and T. M. Monro, "Bismuth glass holey fibers with high nonlinearity," Opt. Express **12**, 5082–5087 (2004).
11. S. Afshar V., W. Q. Zhang, H. Ebendorff-Heidepriem, and T. M. Monro, "Small core optical waveguides are more nonlinear than expected: experimental confirmation," Opt. Lett. **34**, 3577–3579 (2009).
12. G. Qin, X. Yan, C. Kito, M. Liao, T. Suzuki, A. Mori, and Y. Ohishi, "Highly nonlinear tellurite microstructured fibers for broadband wavelength conversion and flattened supercontinuum generation," J. Appl. Phys. **107**, 43108–43111 (2010).
13. F. Poletti, X. Feng, G. M. Ponzo, M. N. Petrovich, W. H. Loh, and D. J. Richardson, "All-solid highly nonlinear singlemode fibers with a tailored dispersion profile," Opt. Express **19**, 66–80 (2011).
14. S. Afshar V. and T. M. Monro, "A full vectorial model for pulse propagation in emerging waveguides with subwavelength structures part I: Kerr nonlinearity," Opt. Express **17**, 2298–2318 (2009).
15. M. D. Turner, T. M. Monro, and S. Afshar V., "A full vectorial model for pulse propagation in emerging waveguides with subwavelength structures part II: Stimulated raman scattering," Opt. Express **17**, 11565–11581 (2009).
16. W. Q. Zhang, M. A. Lohe, T. M. Monro, and S. Afshar V., "Nonlinear self-flipping of polarization states in asymmetric waveguides," IEEE Photon. Technol. Lett. **24**, 1453–1456 (2012).
17. L. Vivien, S. Laval, B. Dumont, S. Lardenois, A. Koster, and E. Cassan, "Polarization-independent single-mode rib waveguides on silicon-on-insulator for telecommunication wavelengths," Opt. Commun. **210**, 43–49 (2002).
18. W. Q. Zhang, M. A. Lohe, T. M. Monro, and S. Afshar V., "Nonlinear polarization self-flipping and optical switching," in "Proceedings of the International Quantum Electronics Conference and Conference on Lasers and Electro-Optics Pacific Rim 2011," (OSA 2011), paper C370.
19. S. Afshar V., M. A. Lohe, W. Q. Zhang, and T. M. Monro, "Full vectorial analysis of polarization effects in optical nanowires," Opt. Express **20**, 14514–14533 (2012).
20. S. Afshar V., W. Zhang, and T. M. Monro, "Experimental confirmation of a generalized definition of the effective nonlinear coefficient in emerging waveguides with subwavelength structures," in "Proceedings of the Conference on Lasers and Electro-Optics/International Quantum Electronics Conference 2009," (OSA 2009), OSA Technical Digest (CD), paper CThBB6.
21. W. Q. Zhang, M. A. Lohe, T. M. Monro, and S. Afshar V., "Nonlinear polarization bistability in optical nanowires," Opt. Lett. **36**, 588–590 (2011).

1. Introduction

Waveguides with high index contrast or sub-wavelength features have recently attracted significant interest due to their extreme nonlinearity and possible applications for photonic devices for optical data processing. Examples of these waveguides are used in three research fields: silicon photonics [1–5], chalcogenide photonics [6–8], and soft glass microstructured photonic devices [9–13]. These waveguides operate in the strong guidance regime and hence theoretical models based on weakly guiding approximations, which consider purely transverse propagating modes (referred to as scalar models in this paper), cannot accurately describe the nonlinear processes in these waveguides.

Recently, a full-vectorial theory of nonlinear interactions in high index and sub-wavelength waveguides has been developed [14]. This new theory has been used to develop models for Kerr nonlinearity [14], Raman effects [15], and nonlinear interaction of two polarizations [19] in the strong guidance regime. The model for Kerr nonlinearity predicted a significantly higher effective nonlinear coefficient γ than the one predicted by scalar models. This has been confirmed experimentally [20].

Through developing a full vectorial model for nonlinear interactions of the two polarizations in high index contrast or subwavelength waveguides, we have shown that there are new unstable solutions of the coupled nonlinear Schrödinger equations, which lead to self-polarization flipping [19, 21]. The cause of this nonlinear self-polarization flipping (NSPF) is the anisotropy of the nonlinear coefficients of the two polarizations that originates from the asymmetry of the waveguide structure (see [19] for a full discussion). It has recently been predicted that the required power for NSPF can be reduced to watt levels in waveguides with only one 2-fold symmetry axis or no symmetry (in this paper, referred to as reduced symmetry), such as rib waveguides, where the birefringence of the two polarizations can be engineered through the

#222244 - $15.00 USD Received 5 Sep 2014; accepted 13 Oct 2014; published 31 Oct 2014

waveguide structure to be close to zero at certain wavelengths, i.e., at zero birefringence wavelength [16]. These predictions were based on an ideal waveguide, where waveguide loss and dispersion were ignored and only continous wave (CW) and noiseless fields were considered.

Here, we investigate NSPF in silicon waveguides with realistic parameters so that it can be tested experimentally, which account for loss, noise and dispersion. We investigate the influences of waveguide structural variations on the flipping behavior, extending our previous formulation to include the loss in the waveguide and investigate its effects, study numerically NSPF behavior for pulsed lasers, where dispersion becomes important, and also examine the effects of fluctuations in the laser power and polarization states on NSPF. We show that silicon rib waveguides with realistic fabricated parameters can lead to polarization switching using few tens of watts peak power pulses with widths as short as 60 ps and laser noise level of order of 7%.

2. Zero birefringence wavelength

The nonlinear interaction of the two polarizations can be described by the following coupled nonlinear Schrödinger equations, which have been generalized to include the loss effects (see the lossless version Eq. (10) in [19]):

$$\begin{aligned}
\frac{\partial A_1}{\partial z}+\sum_{n=1}^{\infty}\frac{i^{n-1}}{n!}\beta_1^{(n)}\frac{\partial^n A_1}{\partial t^n} &= -\frac{\alpha_1}{2}A_1+i(\gamma_1|A_1|^2+\gamma_c|A_2|^2)A_1+i\gamma_c^{'}A_1^*A_2^2\exp(-2iz\Delta\beta),\\
\frac{\partial A_2}{\partial z}+\sum_{n=1}^{\infty}\frac{i^{n-1}}{n!}\beta_2^{(n)}\frac{\partial^n A_2}{\partial t^n} &= -\frac{\alpha_2}{2}A_2+i(\gamma_2|A_2|^2+\gamma_c|A_1|^2)A_2+i\gamma_c^{'}A_2^*A_1^2\exp(2iz\Delta\beta),
\end{aligned} \tag{1}$$

where α_j and $\beta_j^{(n)}$, $j=1,2$ are the absorption and $n-$th order dispersion coefficients of the two polarization modes, $A_j(z,t)$ are the amplitudes of the two polarization fields, $\Delta\beta=\beta_2-\beta_1$ is the birefringence, and $\gamma_{1,2}$, γ_c and $\gamma_c^{'}$ are the effective nonlinear coefficients corresponding to self-phase modulation, cross phase modulation, and coherent phase mixing, respectively (see [19] for derivations and the equations for different γ's). In previous work, Equations (1) for continuous laser fields and lossless waveguides lead to the following coupled dimensionless equations:

$$\begin{aligned}
\dot{v}&=\frac{dv}{d\tau}=v(1-v)\sin\theta,\\
\dot{\theta}&=\frac{d\theta}{d\tau}=-a+2bv+(1-2v)\cos\theta.
\end{aligned} \tag{2}$$

Here $v=P_1/P_0$, $\theta=2z\Delta\beta+2\phi_1-2\phi_2$, $\tau=2P_0\gamma_c^{'}z$ and the parameters a,b are given by:

$$a=-\frac{\Delta\beta}{P_0\gamma_c^{'}}-\frac{\gamma_c-\gamma_2}{\gamma_c^{'}},\quad b=\frac{\gamma_1+\gamma_2-2\gamma_c}{2\gamma_c^{'}},$$

where, $P_i(z)$, and $\phi_i(z)$, $i=1,2$, are the powers and phases of each polarization, respectively, $P_0=P_1+P_2$ is the total power, which is constant in τ. The parameter b depends only on waveguide properties, but a depends on the linear birefringence and total power. Previously we showed that Eqs. (2) have unstable and periodic solutions for $v(\tau)$ and $\cos(\theta/2)$, when $1<a<2b-1$, which result in the nonlinear polarization switching. The required power P_0 for existence of such unstable solutions is restricted by the following inequalities [19]:

$$\gamma_c+\gamma_c^{'}-\gamma_1<\frac{\Delta\beta}{P_0}<\gamma_2-\gamma_c-\gamma_c^{'}. \tag{3}$$

#222244 - $15.00 USD Received 5 Sep 2014; accepted 13 Oct 2014; published 31 Oct 2014

P_0 is usually too high for typical waveguides unless $\Delta\beta$ is small. By carefully designing the waveguide structure, the birefringence can be reduced close to zero and hence the necessary power level P_0 can be reduced. However, in symmetric non-birefringent waveguides such as circular or square waveguides, the condition $\Delta\beta \to 0$ occurs when $\Delta\gamma = (\gamma_2 - \gamma_1) \to 0$ as well, for which Eqs. (2) have only stable solutions and do not show any NSPF behavior. For structures with reduced symmetry, the condition $\Delta\beta \to 0$ can be achieved, while having $\Delta\gamma \neq 0$, at a specific wavelength called zero-birefringence wavelength (ZBW) [17]. At ZBW the two polarization modes have the same β but different field distributions.

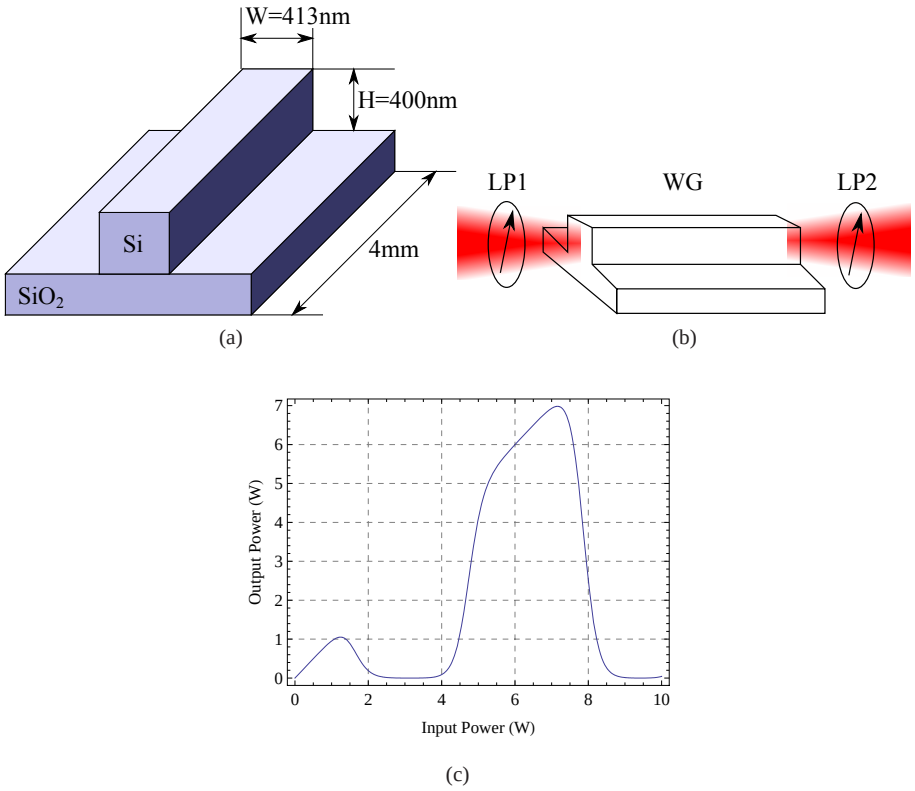

Fig. 1: (a) An example of a optical waveguide with reduced symmetry as defined in the Section 1. (b) Schematics of the experiment setup used throughout this paper. WG: waveguide, LP1&LP2: linear polarizers with polarization aligned 45° to the horizon. (c) Output versus input power for the waveguide in (a) and the experimental setup schematic in (b).

Here, we consider an example of a silicon waveguide with reduced symmetry as shown in Fig.1(a). A rectangular silicon waveguide, which exhibits high birefringence, sits on the top of a silica layer surrounded by air. This kind of asymmetry usually results in a large birefringence, $\Delta\beta$ of the two polarization modes. However, for certain waveguide widths and heights, in the case of Fig.1(a): width 413 nm and height 400 nm, the fundamental modes of the waveguide, TE and TM, become non-birefringent, $\Delta\beta = 0$, at 1550 nm wavelength. At this ZBW, the vertical and the horizontal polarization modes have different mode field distributions, which leads to different nonlinear coefficients along the two polarization directions and NSPF behavior. Throughout this paper, we consider the schematic shown in Fig.1(b) for our simulation; a linearly polarized light is incident on the waveguide. The input state of polarization makes an

#222244 - $15.00 USD Received 5 Sep 2014; accepted 13 Oct 2014; published 31 Oct 2014

angle of 45° with the principal axes of the waveguide. A polarizer aligned with the input polarization state is used after the waveguide to examine the polarization state of the output light. Using Eq. (2) and the procedure explained in detail in [16], figure 1(c) shows the output power as a function of the input power for a CW laser beam and for the waveguide and configuration shown in Fig. 1(a) and 1(b). The output power drops to zero at input power higher than 2.2 W and lower than 3.8 W, indicating that at this input power the state of the polarization has flipped by 90°.

Generally, many waveguides with different heights and widths can have zero-birefringence at one wavelength. Figure 2 shows the two-dimensional contour plot of the difference of the effective refractive indices of the two polarization modes at 1550 nm, $\Delta n_{\text{eff}} = \frac{\lambda}{2\pi}\Delta\beta$ as a function of waveguide width and height, in which the black line represents $\Delta n_{\text{eff}} = 0$. A linear fit of the black line gives the following relation:

$$W\ (\text{nm}) = 1.002 \times H\ (\text{nm}) + 12.4065(\text{nm}). \tag{4}$$

where W and H are the width and height of the Si rib of the waveguide as shown in Fig.1.

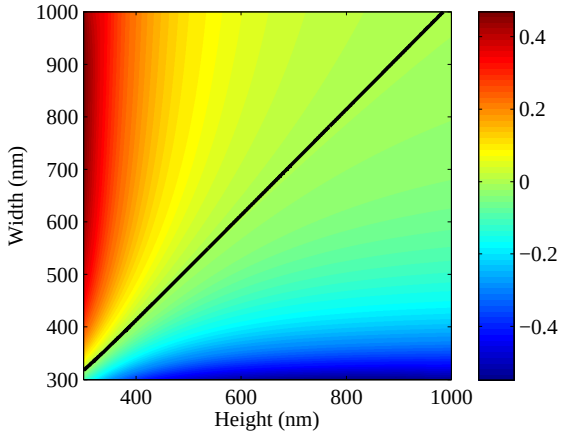

Fig. 2: Difference in the refractive indices of TE and TM for a range of waveguides at 1550 nm. Black line: the contour where $\Delta n_{\text{eff}} = 0$.

It is important to know that in practice, due to unavoidable fabrication distortions, one cannot obtain a waveguide with exactly zero birefringence. However, as long as $\Delta\beta$ is small, the power required for NSPF can be kept to a reasonable level, e.g., in the examples in this paper, the peak power of pulses can be as low as 40 W.

Apart from the power required for NSPF, the flipping period and speed are also closely related to Δn_{eff} [16]. Hence, when designing a practical waveguide for testing in experiment, it is important to know the tolerance of the experiment to fabrication distortion. Due to fabrication errors, the $\Delta\beta$ of the waveguide is no longer zero at the wavelength that it is originally designed for. However, zero-birefringence can still be found in the waveguide at a different wavelength. The zero-birefringence wavelength (λ_{ZB}) of a waveguide is a function of the waveguide's height and width. We define two variables, B and L as shown below, to quantify the change in $\Delta\beta$ and λ_{ZB} due to fabrication distortion:

$$B(W,\lambda) = \frac{\partial\Delta\beta}{\partial H} \qquad L(W,\lambda) = \frac{\partial\lambda_{\text{ZB}}}{\partial H}.$$

#222244 - $15.00 USD Received 5 Sep 2014; accepted 13 Oct 2014; published 31 Oct 2014

For any given waveguide width W and wavelength λ, the variables B and L quantify how much $\Delta\beta$ and λ_{ZB} change for every unit change of waveguide height (H), respectively. Here, we study these two parameters at the specific points $\lambda = 1550$ nm and H given by Eq. (4).

We assume an arbitrary maximum acceptable change in $\Delta\beta$ of 1000 m^{-1} (equivalent to $\Delta n_{\mathrm{eff}} \approx 2.5\times10^{-4}$) and a maximum acceptable change in λ_{ZB} of 500 nm (i.e., a laser with wavelength tunability about 500 nm), then the corresponding allowable change in the waveguide height ΔH_{max} can be found through the following relations respectively:

$$\Delta H_{\mathrm{max,B}} = \frac{1000}{B(\lambda_0)}, \tag{5}$$

$$\Delta H_{\mathrm{max,L}} = \frac{500}{L(\lambda_0)}. \tag{6}$$

By calculating ΔH_{max} for a range of waveguides with width from 300 to 2000 nm, see Table 1, the following trends can be observed: for the same amount of change in $\Delta\beta$, larger waveguides have better tolerance to structural distortion. However, on the contrary, for the same amount of change in λ_{ZB}, smaller waveguides have better tolerance.

Table 1: Comparison of tolerances for different waveguide widths

WG Width (nm)	300	400	500	600	800	1000	1500	2000
$\Delta H_{\mathrm{Max,B}}$ (nm)	0.005	0.145	0.342	0.684	2.03	4.74	21.9	67.6
$\Delta H_{\mathrm{Max,L}}$ (nm)	18.1	6.22	4.26	3.55	3.00	2.78	2.55	2.54

The two trends are inversely related. It indicates that in order to compensate for fabrication distortion, one of two methods can be used: (1) make small waveguides and search for zero birefringence through probing the waveguide using lasers at different wavelengths; (2) make the waveguide large enough such that the fabrication distortion will not lead to significant birefringence. However, by considering other practical issues such as multimodeness, we prefer to use small waveguides (e.g., $W = 413$ nm) for this work.

3. Effects of loss

Apart from fabrication distortion, the loss in the waveguide is also an important property that influences the behavior of NSPF. In the previous study [16], the waveguide loss was ignored and hence the total propagating power P_0 was constant in z, i.e., $\partial P_0/\partial z = 0$. However, the presence of waveguide losses causes an exponential decay of P_0. Here, we investigate, analytically and numerically, the influence of the propagation loss of the two polarizations on NSPF.

We substitute A_j, $j = 1,2$ as $A_j(z) = \sqrt{P_j(z)}\exp(-\frac{\alpha_j}{2}z + i\phi_j(z))$, where P_1, P_2 are the powers and α_1, α_2 are the loss coefficients of the two polarization modes. In Eqs. (1), we ignore the dispersion terms and rewrite Eqs. (1) as:

$$\begin{aligned}
\frac{\partial P_1}{\partial z} &= 2P_1P_2\exp(-z\alpha_2)\gamma_{\mathrm{c}}'\sin\theta,\\
\frac{\partial P_2}{\partial z} &= -2P_1P_2\exp(-z\alpha_1)\gamma_{\mathrm{c}}'\sin\theta,\\
\frac{\partial \phi_1}{\partial z} &= \exp(-z\alpha_1)\gamma_1P_1 + \exp(-z\alpha_2)(\gamma_{\mathrm{c}} + \gamma_{\mathrm{c}}'\cos\theta)P_2,\\
\frac{\partial \phi_2}{\partial z} &= \exp(-z\alpha_2)\gamma_2P_2 + \exp(-z\alpha_1)(\gamma_{\mathrm{c}} + \gamma_{\mathrm{c}}'\cos\theta)P_1,
\end{aligned} \tag{7}$$

#222244 - $15.00 USD Received 5 Sep 2014; accepted 13 Oct 2014; published 31 Oct 2014

in which $\theta = 2z\Delta\beta + 2\phi_1 - 2\phi_2$. In order to analyze these equations further, we consider the special case $\alpha_1 = \alpha_2 = \alpha$, and define $v = P_1/P_0$, we find:

$$\begin{aligned} \frac{\partial v}{\partial \tau} &= (1-v)v\sin\theta, \\ \frac{\partial \theta}{\partial \tau} &= -a(\tau) + 2bv + (1-2v)\cos\theta. \end{aligned} \tag{8}$$

where the independent variable τ is defined by

$$\tau = 2P_0\gamma_c^{'}\left[\frac{1-\exp(-\alpha z)}{\alpha}\right], \tag{9}$$

and

$$a(\tau) = \frac{\gamma_2 - \gamma_c}{\gamma_c^{'}} - \frac{2\Delta\beta}{2P_0\gamma_c^{'} - \alpha\tau}, \quad b = \frac{\gamma_1 + \gamma_2 - 2\gamma_c}{2\gamma_c^{'}}. \tag{10}$$

Equations (8) have the same form as the lossless case Eqs. (2), except that τ is redefined as in Eq. (9) and a is a function of τ and depends on α. There are no analytical solutions to Eqs. (8). However, we can approximate $a(\tau)$ as a step function in τ, i.e., we can consider a split-step scenario such that within a short propagation length the effect of loss is negligible, in which case $a(\tau)$ is constant over this short length. Hence, the NSPF properties in a lossy environment can be reduced to the study of these properties in each discrete section with a slightly different parameter a. Hence, the solutions of lossless waveguides, discussed in [19], can be used to find and analyze the exact solution within each section to any required accuracy. It is necessary therefore to maintain the condition $1 < a(\tau) < 2b-1$ in order to preserve the NSPF property, which requires that α, as well as the length of each section to be small.

In the previous section, we mentioned the importance of reducing $\Delta\beta$ in order to reduce the pump power required for observing NSPF. It is clear from Eq. (10), that a becomes independent of τ and α, in the limit of $\Delta\beta \to 0$. As a result, in this limit, the solutions of Eqs. (8) are the same as those of Eqs. (2), except that τ is now given by Eq. (9) rather than $\tau = 2P_0\gamma_c^{'}z$ as in Eq. (2). This leads to a scaling rule for the NSPF; the solutions $v(\tau)$ and $\theta(\tau)$ remain the same for different values of loss α, if τ in Eq. (9) is kept the same by appropriately scaling up or down the propagation length z and total power P_0. The same property holds if $\Delta\beta$ is not exactly zero but small, i.e., $\Delta\beta << P_0\gamma_c^{'}z$. To demonstrate this, we consider a rib waveguide with $\Delta\beta = 1\ m^{-1}$, $\gamma_1 = 166.5\ W^{-1}m^{-1}$, $\gamma_2 = 173.2\ W^{-1}m^{-1}$, $\gamma_c = 79.77\ W^{-1}m^{-1}$ and $\gamma_c{'} = 35.05\ W^{-1}m^{-1}$ and use a split-step Fourier method to solve the coupled differential equations, Eqs. (1), for CW laser fields and including waveguide loss.

We also consider the configuration in Fig. 1(b), where a linearly polarized beam (with angle 45° between the two polarizations) is incident on the waveguide. Figures 3(a)–3(d) show the total output power as a function of total input power for $\alpha_1 = \alpha_2$, Fig. 3(a) and 3(c), and $\alpha_1 \neq \alpha_2$, Fig. 3(b) and 3(d). All the figures show behavior similar to Fig. 1(c); the output power drops to zero as the input power increases, which indicates that the state of polarization has flipped by 90°. The scalability rule is also apparent; the same output-input behavior is observed by simultaneously decreasing the waveguide length and increasing the input power by the same factor that the loss value increases.

4. Effects of noise

The noise existing in the laser beams is another practical parameter that can affect the behavior of NSPF. The noise exists in both the amplitude and phase of the laser beams, which leads to the noise in the laser power and state of polarization. To investigate the effects of noise on NSPF

#222244 - $15.00 USD Received 5 Sep 2014; accepted 13 Oct 2014; published 31 Oct 2014

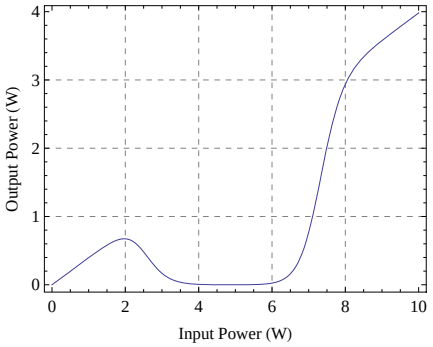

(a) $\alpha_1 = \alpha_2 = \alpha = 100$ dB/m, $L = 40$ mm, $P_0 = 0$ to 10 W

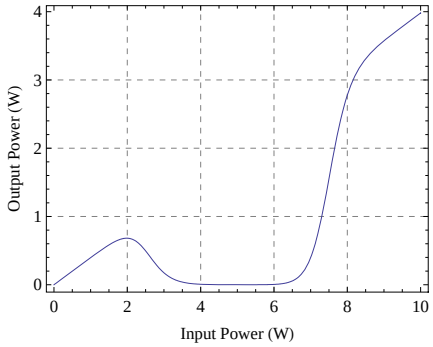

(b) $\alpha_1 = 100$ dB/m, $\alpha_2 = 120$ dB/m, $L = 40$ mm, $P_0 =$ 0 to 10 W

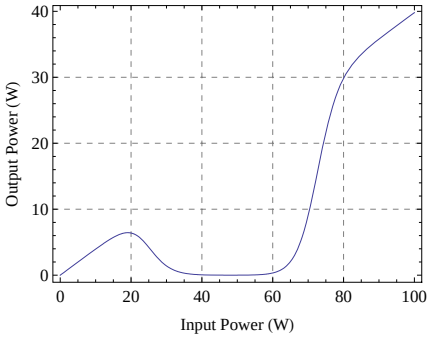

(c) $\alpha_1 = \alpha_2 = \alpha = 1000$ dB/m, $L = 4$ mm, $P_0 = 0$ to 100 W

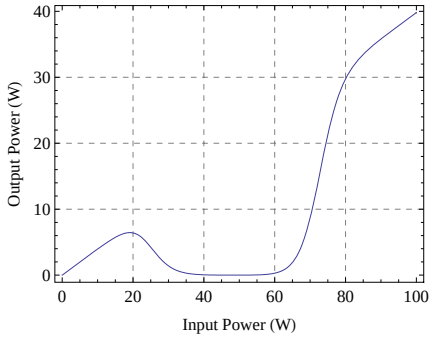

(d) $\alpha_1 = 1000$ dB/m, $\alpha_2 = 1200$ dB/m, $L = 4$ mm, $P_0 = 0$ to 100 W

Fig. 3: The scalability NSPF in lossy systems. (a), (c): the loss in the two polarizations are set to be the same. (b), (d): the loss in the two polarizations are slightly different.

behavior, we incorporate the noise into the amplitude and the phase of input fields of the two polarizations at the beginning of the waveguide as

$$\begin{aligned} A_1^{'}(z=0,t) &= A_1(z=0,t)\exp(i\phi_1) + \varepsilon_1(t)\exp(i\psi_1(t)), \\ A_2^{'}(z=0,t) &= A_2(z=0,t)\exp i(\phi_2) + \varepsilon_2(t)\exp(i\psi_2(t)), \end{aligned} \tag{11}$$

where A_1, A_2, ϕ_1 and ϕ_2 ($\phi_1 = \phi_2$ for linearly polarized input laser) are the noiseless amplitudes and phases of the input fields of the two polarizations, respectively, and $\varepsilon_1(t)\exp(i\psi_1(t))$ and $\varepsilon_2(t)\exp(i\psi_2(t))$ are the noises in the two polarizations. The power of the noise terms, $|\varepsilon_1(t)|^2$, $|\varepsilon_2(t)|^2$ are randomly distributed within the interval of $\left[0, x|A_j(t)|^2\right)$, $j = 1,2$, where x is a free parameter that represents the percentage of the power in each polarization. The two phase noise terms, $\psi_1(t)$ and $\psi_2(t)$, are also randomly distributed within $[0, 2\pi)$. We then use a split-step Fourier method to numerically solve the coupled nonlinear Schrödinger equations, Eqs. (1), with the initial condition as in Eqs. (11). We ignore the dispersion terms in Eqs. (1), however, we consider quasi-CW pulses (pulses that are much longer than the length of the waveguide) in order to compare the results with those of the next section, where we include the dispersion

#222244 - $15.00 USD Received 5 Sep 2014; accepted 13 Oct 2014; published 31 Oct 2014

effects. We consider super Gaussian and quasi-CW pulses of the form:

$$A_1(z=0,t) = A_2(z=0,t) = \sqrt{\frac{P_0}{2}} \exp\left[-\frac{1}{2}\left(\frac{t}{t_0}\right)^{2m}\right],$$

where $t_0 = 5$ ns is the pulse width. We choose the peak power (P_0) of the input pulse as $P_0 = 40$ W, since at this power the polarization is switched off for noiseless CW input power as shown by the red dot point in Fig. 4(a). The noise level x is varied from 0 to 100%. We also consider the same experimental setup as in Fig. 1(b), however, with realistic length and the loss values of typical silicon waveguides, i.e., $L = 4$ mm and $\alpha = 10$ dB/cm (we picked a number from the high end, a smaller loss will be even better). We have examined the output pulse as the noise level x is increased from 0% (noiseless) to 20%. For every x value, the output pulse was calculated for an input pulse with random amplitudes and phases as a function of time, as in Eqs. (11). Figures 4 (b)–4(d) show the results. In every figure, blue and green data points correspond to the input and output pulse at different times, respectively. Since the case in Fig. 4(b) does not contain noise, its behavior should follow the theoretical prediction exactly. This is confirmed by comparing the input and output power at the center of the pulse ($t = 0$) with those of the CW input power at 40 W, shown by the red dot in Fig. 4(a). As the noise increases, the polarization fluctuation of the propagating pulse also increases, which is shown in the form of increasing noise in the output.

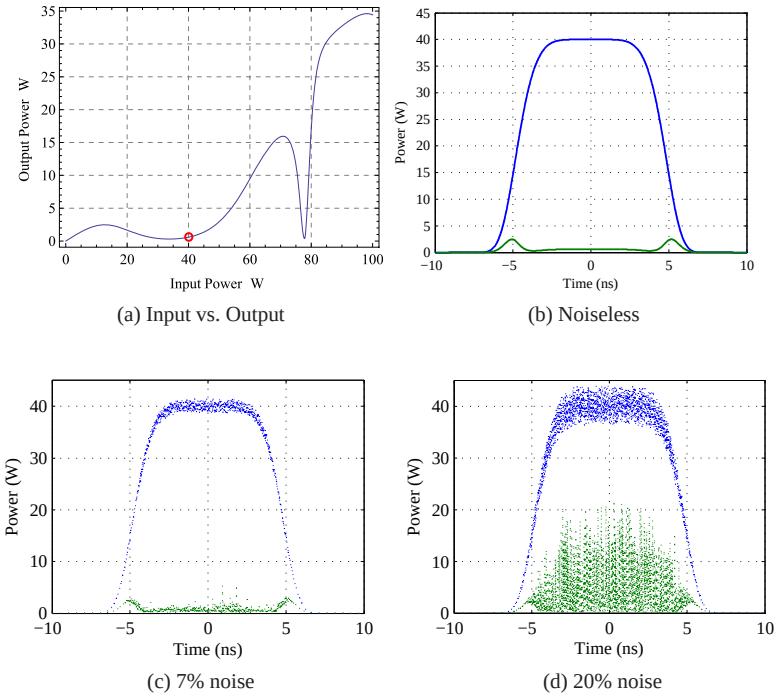

(a) Input vs. Output (b) Noiseless

(c) 7% noise (d) 20% noise

Fig. 4: (a) Analytical prediction of the output versus CW input power of the waveguide in Fig. 1 (a) with $L = 4$ mm, $\alpha = 10$ dB/cm and a CW laser. The red dot is a case where the same input power (40 W) are used in (b)-(d). (b)-(d) The input (blue) and output (green) pulse shape with 0%, 7% and 20% of noise.

#222244 - $15.00 USD Received 5 Sep 2014; accepted 13 Oct 2014; published 31 Oct 2014

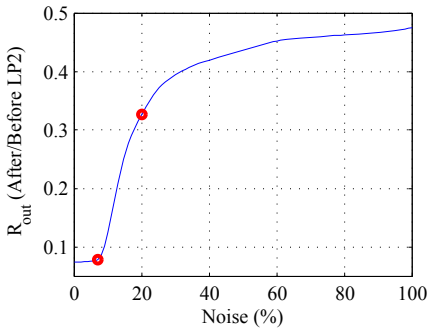

Fig. 5: The influence of noise on the behavior of NSPF with 40 W, 5 ns (T_0) super-Gaussian pulses in a 4 mm long waveguide. The red dots represent the ratio at 7% and 20% noise level.

In addition to examining the temporal profiles of the input and output pulses, we have also calculated the ratio of output to input pulse energy, R_{out}, as a function of noise level x, as shown in Fig. 5. Small values of R_{out},corresponding to low noise level, indicate that most of the input energy of the pulse has been blocked by the output polarizer LP2, which is the result of polarization flipping in the waveguide. As x increases and R_{out} asymptotically approaches 0.5, almost half of the input pulse energy goes through the polarizer which indicates that the output pulse is fully depolarized. Figure 5 suggests that the noise level of up to 7% does not significantly affect NSPF behavior, for the specific waveguide considered in this example. Note that the typical noise level of commercial laser systems is around 5% to 10%.

5. Effects of dispersion

In our previous model of the nonlinear interaction of two polarizations [19], we ignored the temporal dependence of the pulses or dispersive effects. However, in practice, pulsed lasers are required to achieve high peak powers. In such cases, the dispersion of the waveguide becomes important and must be considered in order to correctly describe NSPF behavior. We start with Eqs. (1) and transform them into the Fourier domain to obtain:

$$\begin{aligned}
\frac{\partial A_1(\omega)}{\partial z} &= -\frac{\alpha_1}{2}A_1(\omega) + i\beta_1(\omega)A_1(\omega) + i\left(\gamma_1 |A_1(\omega)|^2 + \gamma_c |A_2(\omega)|^2\right)A_1(\omega) \\
&\quad + i\gamma_c' A_1^*(\omega)A_2^2(\omega)\exp(-2iz\Delta\beta), \\
\frac{\partial A_2(\omega)}{\partial z} &= -\frac{\alpha_2}{2}A_2(\omega) + i\beta_2(\omega)A_2(\omega) + i\left(\gamma_2 |A_2(\omega)|^2 + \gamma_c |A_1(\omega)|^2\right)A_2(\omega) \\
&\quad + i\gamma_c' A_2^*(\omega)A_1^2(\omega)\exp(2iz\Delta\beta),
\end{aligned} \tag{12}$$

where $\beta_n(\omega)$ $n = 1,2$ are the propagation constants of the fundamental modes of the waveguide at the frequency ω, $\Delta\beta = \beta_1(\omega_0) - \beta_2(\omega_0)$ and ω_0 is the central frequency of the input pulse which in this case is $\omega_0 = 2\pi c/\lambda_0$ where c is the speed of light and $\lambda_0 = 1550$ nm. The advantage of writing the coupled nonlinear Schrödinger equations in the frequency domain, as in Eqs. (12), is that $\beta_1(\omega)$ and $\beta_2(\omega)$ include the full dispersion of the two polarizations rather than only a few dispersion orders (as in Eq. (1)). We have solved Eqs. (12) numerically, using a Fourier split step method, for the waveguide shown in Fig. 1. The propagation constants of the waveguide are calculated by using a finite element package (COMSOL). For this waveguide, the group velocity dispersion of both polarizations are anomalous at the pump wavelength. To

#222244 - $15.00 USD Received 5 Sep 2014; accepted 13 Oct 2014; published 31 Oct 2014

confirm the validity of our numerical model, we have first considered the results of the numerical model for quasi-CW pulses, with a very narrow line width, and confirm that they match the analytical results of the CW model in [19], see Fig. 4 (a).

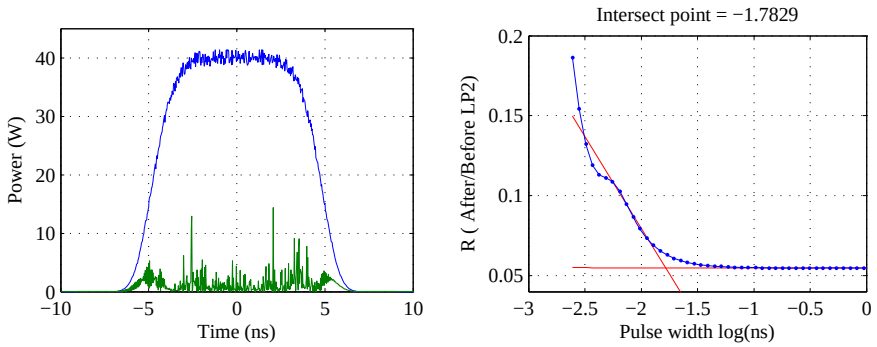

(a) 5 ns (T_0), 7% noise 10 and 12 dB/cm loss

(b) Noiseless, 10 dB/cm loss

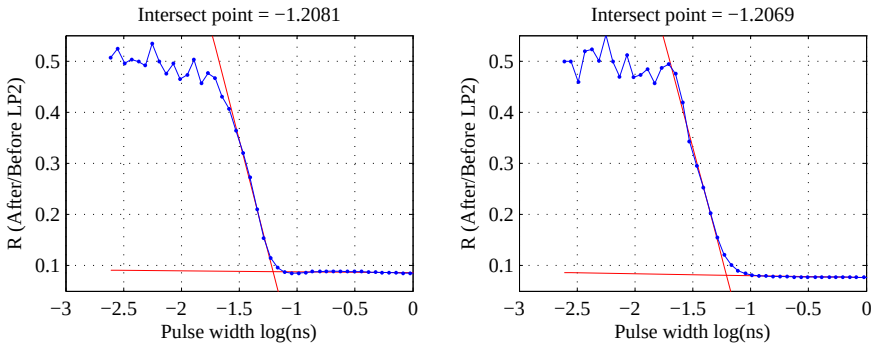

(c) 7% noise, 10 dB/cm loss

(d) 7% noise, 10 and 12 dB/cm loss

Fig. 6: The influence of dispersion on the behavior of NSPF. (b-d): The intersections of the red lines define the threshold of pulse width for each case.

The influence of dispersion on NSPF cannot be isolated from that of other parameters such as the noise. Figures 6(b) and 6(c) show the ratio of the input to output pulse energies, R_{out}, as a function of pulsewidth [$\log_{10}$(pulsewidth)] for waveguides with and without laser noise. In both figures, for longer pulses R_{out} approaches an asymptotic value. As the pulsewidth decreases, R_{out} increases quickly indicating that the output pulses are depolarized. We define the intersection between the asymptotic values of R_{out} and a line representing the fast growing section of R_{out} graph (red lines in Figs. 6(b)–6(d)), as the minimum pulsewidth for which NSPF behavior is still observed. It is observed that NSPF behavior can be observed for pulsewidths as low as 16.5 ps for the noiseless case, Fig. 6(b). However, the minimum pulsewidth for which NSPF behavior can be observed, when a noise level of 7% is considered, is of order 62 ps. This can be explained by noticing that the noise in our model is broadband and acts as a seed of some spontaneous nonlinear processes such as four-wave mixing and modulation instability. Figure 6 (d), shows R_{out} as a function of pulsewidth when the loss of the two polarizations are different, 10 and 12 dB/cm. In this case, the minimum pulsewidth is similar to Fig. 6(c) for which the two polarizations have the same loss of 10 dB/cm.

#222244 - $15.00 USD Received 5 Sep 2014; accepted 13 Oct 2014; published 31 Oct 2014

6. Conclusion

We have shown the feasibility of achieving NSPF in fabricable silicon waveguides by investigating the behavior of NSPF in a silicon waveguide with realistic parameters. We have studied the combined effects of structural variation, waveguide loss, laser noise and waveguide group velocity dispersion on NSPF. For every parameter, we have determined the range for which NSPF can be observed. We have shown that NSPF should be observed in a 400 nm silicon waveguide using tunable pulsed lasers with pulse widths bigger than 62 ps, laser noise level lower than 7%, loss of 10 dB/cm and peak power of a few tens of watts.

The study here focused on a typical silicon waveguide structure, shown in Fig. 1, and hence the parameter ranges, for which NSPF can be observed, are specific to the particular waveguide and setup used in this study. The range of these parameters change for other waveguide structures. It would be possible to identify the waveguide structure that optimizes one or more of these parameters.

One important parameter that affects NSPF behavior is the dispersion which is determined by the waveguide geometry (refractive index distribution $n(x,y)$). There may be an optimum dispersion profile for NSPF behavior. However, to investigate this possibility as well as to discover other interesting nonlinear effects, further development of the original full vectorial nonlinear Schrödinger equations is required. Such equations should describe the nonlinear interaction of the two polarizations, to include temporal effects (dispersion), which by itself is a topic for future investigation.

The study here shows that typical silicon waveguides with structures shown in Fig. 1 and with practical parameters can be used for nonlinear polarization switching.

Acknowledgments

We acknowledge the support of the South Australia State Government and the Italian Regional Government for funding this work. Authors Zhang, Lohe, Monro, and Afshar V. also acknowledge ARC funding support (DP110104247). Tanya Monro also acknowledges the support of a Federation Fellowship.